IJCRT.ORG ISSN : 2320-2882

INTERNATIONAL JOURNAL OF CREATIVE RESEARCH THOUGHTS (IJCRT)

An International Open Access, Peer-reviewed, Refereed Journal

Additive Manufacturing: Evolution, Principles, and Industrial Applications

RAJESH KUMAR - SCHOLAR

DR. ANIL KUMAR RAJAK - ASSOCIATE PROFESSOR

DR. SUMIT KUMAR SHARMA - ASSISTANT PROFESSOR

PRIYANKA – SCHOLAR

Abstract

This research investigates the fabrication and characterization of ER-4043 aluminum alloy deposits produced through Wire Arc Additive Manufacturing (WAAM) using a robotic Gas Metal Arc Welding (GMAW) system. Aluminium beads were deposited on an Al 6061-T6 substrate following an L16 orthogonal array, with wire feed rate and travel speed varied as input parameters, while surface roughness, toe angle, bead height, and depth of penetration were evaluated as output responses. A sustainability-based ranking framework was applied to identify the optimal parameter combination, with Alternative 15 yielding the best overall bead quality. Microstructural analysis using optical and scanning electron microscopy revealed an Al-Si eutectic structure with columnar-to-equiaxed grain transition from the molten pool outward, along with minor defects including porosity and a distinct heat-affected zone. XRD confirmed an α-Al dominated matrix with minor β-Al_2CuMg and χ-Mg_2Si intermetallic phases. Porosity analysis showed an average pore area of 79.379 μm², while Vickers microhardness testing revealed a decreasing trend from the bottom (76.6 HV) to the top (73.9 HV) of the deposit, with an average of 75.47 HV. These findings establish process-microstructure-property correlations essential for optimizing WAAM-fabricated aluminum components.

Keywords: Wire Arc Additive Manufacturing (WAAM), ER-4043 Aluminum Alloy, Microstructure, Porosity, Microhardness

1. Introduction

Additive Manufacturing: Evolution, Principles, and Industrial Applications

Three-dimensional (3D) printing, widely known as additive manufacturing (AM), has evolved considerably since its emergence in the 1980s. One of the earliest developments was reported by Dr. Hideo Kodama, who filed a patent for a 3D printing technique in Japan in 1981. Subsequently, Dr. Charles Hull introduced the term **stereolithography (SLA)** and established 3D Systems Corporation in 1986, significantly contributing to the development and commercialization of SLA technology. During the 1990s, several AM technologies, including **fused deposition modeling (FDM)** and **selective laser sintering (SLS),** were developed and initially employed primarily for rapid prototyping and product development.

With the advancement of the technology in the early 2000s, AM expanded beyond prototyping into high-value industrial sectors such as aerospace, healthcare, and automotive manufacturing. The development of metal-based processes, particularly **direct metal laser sintering (DMLS)** and **electron beam melting (EBM),** further broadened the scope of AM by enabling the fabrication of functional metallic components. According to the ASTM F42 Technical Committee, additive manufacturing is defined as a process of joining materials to produce objects from three-dimensional model data, generally in a layer-by-layer manner, in contrast to conventional subtractive manufacturing approaches [1]. AM is also referred to by terms such as solid freeform fabrication, direct digital manufacturing, layer manufacturing, additive fabrication, and rapid manufacturing. In a broader context, AM encompasses manufacturing approaches capable of producing prototypes, tools, patterns, and functional components with properties suitable for direct industrial applications.

A wide variety of materials can be processed using AM, including metallic alloys, thermoplastics, thermosetting polymers, ceramics, and composite materials, depending on the specific process and intended application. Although AM is relatively recent compared with conventional manufacturing technologies, it represents one of the most versatile manufacturing approaches because of its ability to fabricate geometrically complex components directly from digital models. Its application has expanded rapidly into several industries, including aerospace, automotive, healthcare, dentistry, heavy machinery, oil and gas, railways, marine engineering, and consumer products [2]. AM initially gained widespread acceptance in aerospace and medical applications because of its ability to produce lightweight and customized components. Compared with subtractive processes such as milling, AM generally provides greater geometric freedom and can significantly reduce material wastage. Furthermore, unlike conventional forming and molding processes, 3D printing generally does not require dedicated molds or hard tooling for producing individual components. Consequently, AM is particularly attractive for applications involving complex geometries, low production volumes, rapid product development, and situations where conventional tooling involves substantial cost and lead time.

The role of AM has now extended well beyond its original application in rapid prototyping. The technology has become increasingly established for producing tooling, fixtures, molds, and functional components used in conventional manufacturing operations. Moreover, manufacturers are progressively adopting AM for large-scale production. The greatest potential of AM, however, lies in the development of components specifically designed to exploit the capabilities of additive processing. Rather than simply reproducing conventionally manufactured components, AM enables the realization of geometries and design concepts that may be difficult or impossible to manufacture using traditional methods. The ability to produce geometric complexity without a proportional increase in manufacturing cost allows components and assemblies to be consolidated, lightweighted, and optimized for improved functional performance [3].

Several AM processes have been developed, each based on a specific material-processing mechanism and targeted toward particular applications. In FDM**,** thermoplastic materials are deposited through a heated nozzle in successive layers. SLA employs photopolymer resins that are selectively solidified using ultraviolet radiation. In SLS, a laser selectively fuses powdered materials, whereas binder jetting utilizes a liquid binding agent to selectively join powder particles. Metal-specific processes such as DMLS and EBM employ laser energy and electron-beam energy, respectively, to consolidate metallic feedstock. Material jetting produces components by depositing controlled droplets of material, while PolyJet technology combines inkjet-based deposition with photopolymerization to fabricate components using different materials. These diverse processing capabilities have substantially expanded the application of AM in aerospace, automotive, biomedical, and other advanced engineering sectors.

Another major advantage of AM is its ability to process materials that are difficult to manufacture using conventional cutting, forming, or machining techniques. Materials such as ceramics, titanium alloys, and nickel-based superalloys, including Inconel, can be challenging to process conventionally but can be effectively fabricated using appropriate AM technologies. Furthermore, AM facilitates the development of **multi-material and functionally integrated components**, allowing expensive or high-performance materials to be strategically utilized only in regions where their specific properties are required. The increasing availability of high-performance polymers and polymer composites has also enabled the replacement of conventionally manufactured metallic components with lighter and, in some cases, more economical additively manufactured alternatives.

AM can contribute to sustainable manufacturing by reducing material wastage during component production and enabling **on-demand manufacturing** [4]. Instead of maintaining large inventories of physical components, digital component models can be stored and used for production whenever required. This concept of a digital inventory can reduce storage requirements and minimize the risk of obsolete physical stock. AM also facilitates economical **mass customization**, since components can be individually designed without requiring expensive dedicated tooling. This capability is particularly beneficial for products such as footwear, furniture, hearing aids, dental mouthguards, orthotic devices, and customized medical splints, where individual geometrical modifications can be incorporated without substantially increasing production costs.

Metal additive manufacturing (MAM), commonly referred to as metal 3D printing, is an advanced manufacturing approach in which metallic components are fabricated incrementally from digital three-dimensional models. MAM encompasses several technologies, including DMLS and EBM, which utilize different energy sources and processing mechanisms to consolidate metallic feedstock. In DMLS, a high-power laser selectively melts or sinters metal powder to produce dense and geometrically complex components. In contrast, EBM utilizes a focused electron beam within a vacuum environment to melt and consolidate metallic powder, offering high processing temperatures and the potential for producing components with desirable mechanical properties. MAM has gained significant attention in aerospace, automotive, biomedical, and other high-performance applications because it enables the production of complex geometries, customized components, lightweight structures, and rapidly developed prototypes while potentially reducing material consumption and manufacturing lead time [5]. Continuous advances in feedstock materials, process control, energy sources, and dimensional precision are further expanding the industrial potential of metal additive manufacturing.

2. Literature Review

Ahsan et al. [34] investigated wire-feed additive manufacturing (AM) as an advanced approach for fabricating complex-shaped functional metallic components with improved geometrical accuracy, surface quality, and material properties, particularly for demanding applications in the aerospace, automotive, and rapid tooling sectors. Compared with conventional subtractive manufacturing techniques such as CNC machining, AM offers several advantages. The complete manufacturing sequence, from component design to final fabrication, can be automated through an integrated CAD/CAM system. This significantly reduces human intervention for producing new components and can also decrease overall manufacturing time. Although CNC machining programs can be generated automatically from CAD models, complex geometries often require multiple re-fixturing operations, resulting in additional calibration, setup time, and manufacturing costs.

Sood et al. [77] examined the effect of key Fused Deposition Modeling (FDM) process parameters on the dimensional accuracy of ABSP400 components. The study evaluated the influence of raster angle, layer thickness, air-gap orientation angle, and raster width on the dimensional performance of printed parts. Taguchi's design of experiments, combined with the Grey Taguchi optimization method, was used to identify the optimum parameter settings for minimizing dimensional variations in length, width, and thickness. Their findings revealed that material shrinkage was the dominant factor contributing to dimensional inaccuracies in the fabricated components.

Zhang and Peng et al. [78–83] applied Taguchi-based optimization methods to determine the optimal processing conditions for the FDM process. Their investigation focused on four principal parameters: wire-width compensation, extrusion speed, layer thickness, and filling speed, while dimensional error and warpage were selected as the response variables. Using an L9 orthogonal array, Taguchi analysis, and fuzzy comprehensive evaluation, they concluded that wire-width compensation exerted the greatest influence on the overall performance index, followed sequentially by extrusion speed, layer thickness, and filling speed.

M. D. Barath Kumar et al. [43] presented a comprehensive review of WAAM processes and associated techniques, with particular emphasis on residual stresses, microstructural characteristics, and mechanical properties of as-fabricated and post-processed WAAM components. Their review highlighted that the WAAM process can generate residual stresses, distortion, porosity, and cracking during metallic component fabrication. Various approaches for reducing residual stresses and improving the resultant material properties were also discussed. In powder-feed and powder-bed AM technologies, typical layer thicknesses range from 20–100 µm, while dimensional accuracy can reach approximately 0.05 mm and surface roughness values can be in the range of 9–16 µm. Studies comparing components fabricated using metal wire and powder feedstocks have reported broadly similar microstructural characteristics; however, a greater tendency for porosity was observed in some powder-deposited components.

Thrimurthulu et al. [84–85] investigated optimum component orientation in FDM with the objective of simultaneously improving surface quality and reducing build time. A genetic algorithm was employed to determine the optimum orientation. Two types of geometries, namely an axisymmetric component and a three-dimensional component, were considered. The optimization involved two competing objectives: minimizing build time and maximizing surface finish. The study also incorporated minimization of implicit support structures. A mathematical model was developed to estimate average surface roughness and build time, providing a useful approach for determining the optimum orientation of complex components.

Dharmendra et al. [86] investigated the microstructural characteristics of an additively manufactured nickel–aluminium bronze alloy and reported pronounced grain coarsening near the melt-pool boundary regions. Their observations demonstrated significant microstructural variations within the deposited material. Periodic microstructural heterogeneities, commonly referred to as “layer bands,” were observed near the melt-pool boundary and were associated with the layer-by-layer deposition sequence.

Nie et al. [87] examined the mechanical and metallurgical characteristics of a 4043 aluminium alloy component fabricated using the CMT-based WAAM process. Their results demonstrated that process parameters significantly affect the deposited bead geometry, hardness, surface roughness, and microstructural evolution. These findings highlight the importance of controlling process conditions to achieve consistent geometrical and material characteristics in WAAM-fabricated aluminium components.

Ortega et al. [88] reported that the initial deposited layer exhibited a relatively finer microstructure, which gradually became coarser toward the upper regions of the build. This microstructural evolution was attributed to the relatively low initial temperature of the substrate, which promoted a higher cooling rate during deposition of the first layer. As deposition progressed, heat accumulation increased, resulting in a lower effective cooling rate and consequently promoting grain coarsening in the upper layers.

Langelandsvik et al. [89] reported that WAAM can provide improved mechanical characteristics compared with conventional casting because of the relatively rapid cooling conditions associated with the deposition process. Interestingly, their investigation of ER4043 aluminium alloy fabricated through WAAM revealed relatively low levels of porosity. The study further emphasized that microstructural characteristics and porosity are among the principal factors governing the tensile behaviour of additively manufactured aluminium alloys.

Pramod et al. [90] compared the mechanical performance of components produced using different arc-based welding approaches, including GMAW [65], GTAW [3], and CMT. Among the investigated processes, CMT exhibited superior performance. This behaviour was primarily associated with the relatively controlled heat input of the CMT process. Excessive heat input can increase thermal accumulation and promote defects such as porosity, thereby adversely affecting the mechanical properties of the deposited material.

Liu et al. [91] reported the presence of a considerable fraction of coarse grains in the interface regions of transversely deposited weld beads in thick-walled structures. Grain refinement generally contributes to increased microhardness and improved tensile performance. Consequently, the observed grain coarsening in the transverse direction was associated with comparatively inferior tensile characteristics. However, the relatively small differences in tensile properties between the horizontal and vertical orientations were considered insignificant.

3. Experimental procedure

3.1 Materials and Machine setup

Bead deposition experiments were performed using a Gas Metal Arc Welding (GMAW) system integrated with a 6-axis ABB industrial robot (ABB IRB 1520ID), as illustrated in Figure 14. An ER-4043 aluminium alloy wire with a diameter of 1.2 mm was employed as the filler material, while a 10 mm thick Al-6061 plate served as the substrate. Welding was carried out using a Kemppi KempArc SYN 500 power source operating in the 1-MIG mode. The robotic motion and deposition parameters were programmed using RAPID, ABB's proprietary programming language, and argon was used as the shielding gas throughout the deposition process. Beads were fabricated according to an L16 orthogonal array, with wire feed rate and travel speed selected as the variable process parameters, as summarized in Table 3. The remaining process parameters, including current (50 A), voltage (16 V), shielding gas flow rate (20 L/min), and stand-off distance (15 mm), were maintained constant during all experiments. The upper and lower limits of the input parameters were established through preliminary trial experiments. The deposited beads were characterized using surface roughness (Ra, µm), toe angle (°), bead height (mm), and depth of penetration (mm) as the response variables. Surface roughness was measured using a Mitutoyo Surftest SJ-210 portable surface roughness tester, whereas the toe angle, bead height, and depth of penetration were determined using a toolmaker's microscope.

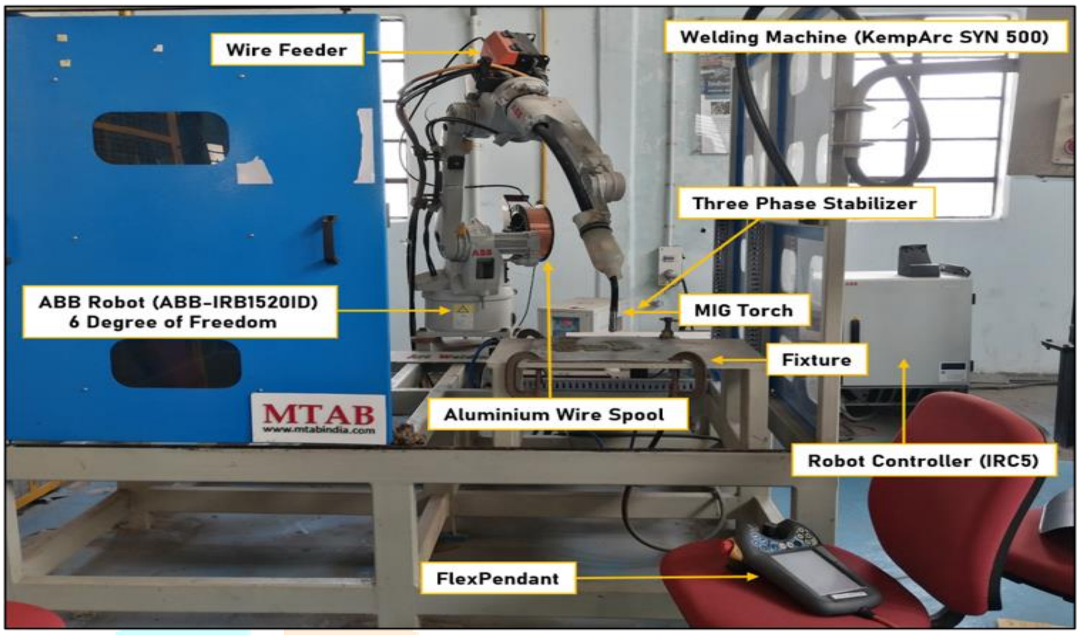

Figure1. Experimental setup of WAAM

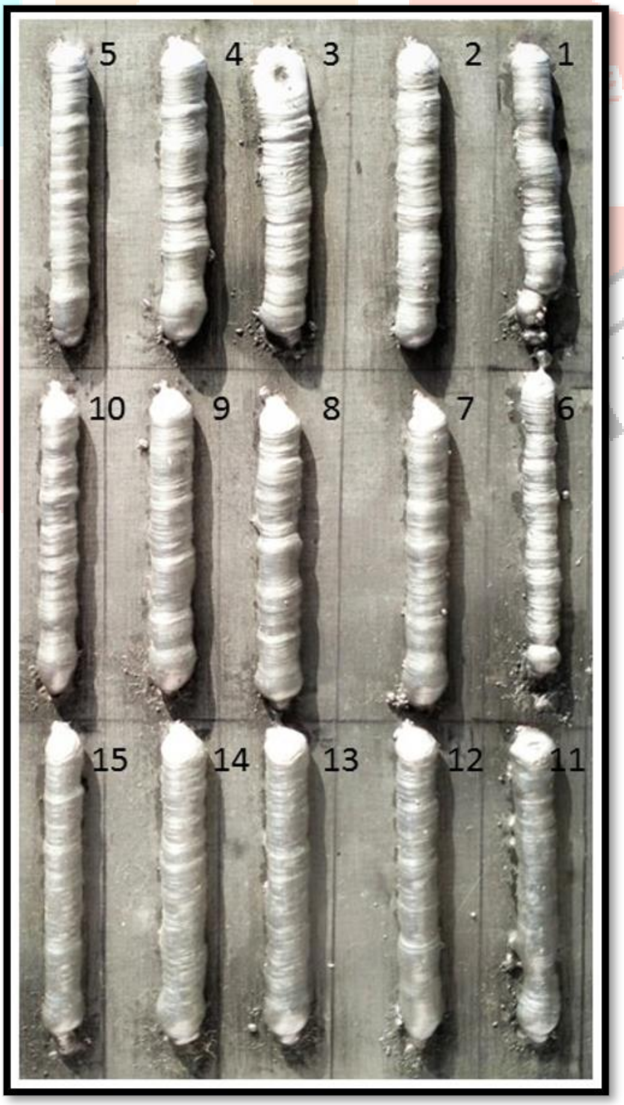

Figure2. Image of deposited bead.

The ER-4043 aluminium alloy deposit was fabricated using the Wire Arc Additive Manufacturing (WAAM) process integrated with a robotic Gas Metal Arc Welding (GMAW) system. The deposition was performed using the fixed process parameters listed in Table 1. Throughout the fabrication process, the wire deposition frequency was maintained at 5 Hz with a 60% duty cycle, while a constant stand-off (working) distance of 13 mm was maintained between the welding torch and the deposited surface to ensure stable arc characteristics and consistent material deposition.

Table 1. Deposition Parameters.

System Technical Specification	Value
Wire Diameter	1.20 mm
Wire feeding rate (mm/s)	9.0
Shielding gas (Ar) flow rate (lpm)	20.0
Contact tip to work piece distance (mm)	15.0
Mode of Operation	Constant frequency 5 Hz, and 60% duty cycle

Material deposition was performed on an Al6061-T6 aluminum alloy substrate plate measuring 100 mm × 100 mm × 20 mm. The chemical composition of both the filler wire and the substrate plate is presented in Table 2. Deposition was carried out to build beads up to a height of 50 mm.

Table 2. Nominal chemical composition (wt. %) of filler wire ER4043 and substrate Al6061-T6.

Alloys	Al	Si	Cu	Mn	Mg	Fe	Cr	Zn	Ti
ER 4043	92.90	5.60	0.30	0.05	0.05	0.80	_	0.10	0.02
Al 6061	97.60	0.71	0.24	0.02	1.00	0.20	0.15	0.06	0.02

Table 3. Experimental design and their output response.

	Input parameter		Output parameter			
S.no	Wire feed rate (m/min)	Welding torch speed (mm/s)	Surface roughness (µm)	Toe angle (degree)	Bead height (mm)	Depth of penetration (mm)
1	7.5	3.0	6.310	80.77	2.09	1.04
2	8.0	3.0	8.937	89.64	2.91	1.91
3	8.5	3.0	11.984	103.16	3.57	2.31
4	9.0	3.0	14.259	120.36	3.88	3.66
5	7.5	3.5	5.392	61.22	3.21	1.51
6	8.0	3.5	7.519	71.64	3.63	2.16
7	8.5	3.5	10.902	85.65	3.74	3.69
8	9.0	3.5	11.982	102.67	4.1	3.89
9	7.5	4.0	3.652	58.95	3.93	2.81
10	8.0	4.0	4.874	61.07	4.01	3.18
11	8.5	4.0	6.891	70.41	4.22	3.68
12	9.0	4.0	9.691	83.69	4.37	4.01
13	7.5	4.5	2.019	46.74	3.95	3.11
14	8.0	4.5	2.931	50.08	4.16	3.45
15	8.5	4.5	4.644	61.14	4.57	3.91
16	9.0	4.5	6.987	68.91	4.62	4.32

3.2 **Materials Characterization**

The polished specimens were chemically etched using Keller's reagent, consisting of 95 mL distilled water (H_2O), 2.5 mL nitric acid (HNO_3), 1.5 mL hydrochloric acid (HCl), and 1.0 mL hydrofluoric acid (HF). The microstructural characteristics of the WAAM-fabricated ER-4043 aluminium alloy specimens produced using robotic GMAW were examined using an optical microscope (Leica DM 2500) and a field-emission scanning electron microscope (FE-SEM, Supra 40, Zeiss SMT AG, Germany). Phase identification of the deposited samples was performed by X-ray diffraction (XRD) using a D8 Advance diffractometer (Bruker AXS, Germany). The microhardness of the deposited beads was measured using an automatic Vickers hardness tester (Mitutoyo HM-200 Autovik) under a load of 0.05 kgf with a 10 s dwell time. Hardness measurements were taken perpendicular to the grain growth direction to evaluate the variation in hardness across the deposited bead from the bottom region to the top region.

4. Results and Discussions

The ranking outcomes were finalized based on a sustainability-driven framework. Benefit and cost criteria for the output responses were selected based on the experimental results, which in turn were governed by the corresponding input parameters. These findings carry significant implications for large-scale manufacturing industries and hold considerable relevance for future applications.

The results summarizes the input parameters along with their corresponding output responses for the WAAM process. Four output criteria: surface roughness, toe angle, bead height, and depth of penetration were evaluated across the different process alternatives, along with the materials characterization in terms of microstructure, porosity, phase analysis, and mechanical properties in terms of hardness has been evaluated at optimized parameter.

4.1 Microstructure Analysis

Figure 3 presents cross-sectional micrographs of the ER-4043 aluminum alloy specimen deposited at a travel speed of 4.5 mm/s, wire feed rate of 8.5 mm/s, and constant current of 50 A. Optical micrographs recorded from top to bottom of the specimen are shown in Figure 17(a, b). The deposited material displays a characteristic Al-Si solidification structure, with grains comprising a dendritic aluminum solid solution separated by an Al-Si eutectic phase. A few minor defects were observed, including porosity, hot cracks, and a heat-affected zone (HAZ). The HAZ was evident as a distinct layer between the substrate and the bead, where the material underwent partial melting without full fusion. The microstructure within this zone differs from that of both the base metal and the weld bead. Notably, the morphology and size of the dendritic structure varied depending on the location within the bead.

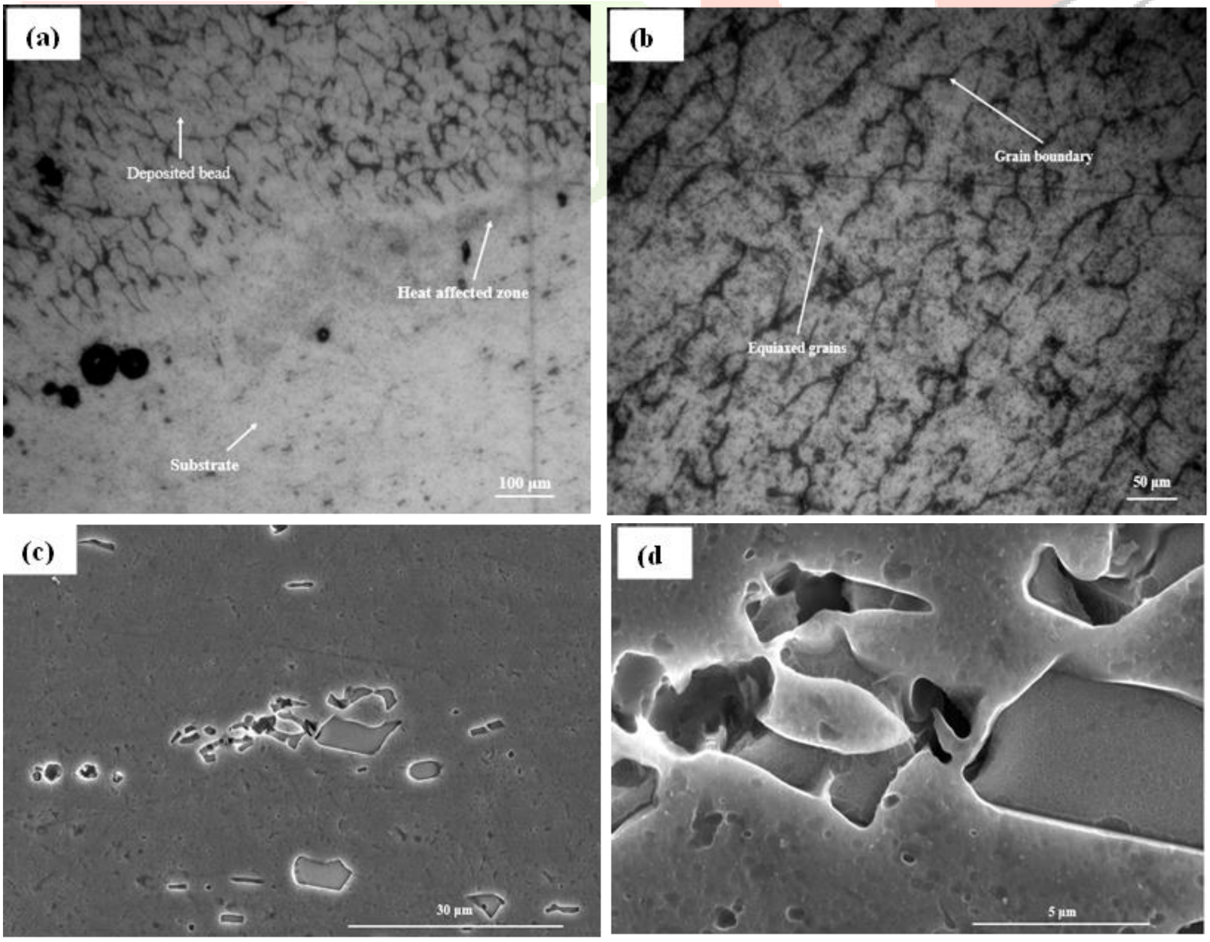

Figure 2. (a-b) is optical micrograph image of the cross section of a bead sample of ER 4043 aluminum alloy, (c-d) Scanning electron micrographs of the cross section of a deposited bead.

High-magnification scanning electron microscopy (SEM) was further employed to examine the grain structure in detail, confirming that the microstructure varies progressively from the top to the bottom of the specimen. These microstructural variations across the deposited bead are governed primarily by the temperature gradient and solidification rate, both of which are strongly influenced by the input process parameters—an important consideration in WAAM processing. Owing to the high solidification rate and steep thermal gradient near the molten pool, grains adjacent to the pool exhibit a columnar morphology, which progressively transitions to an equiaxed structure with increasing distance from the molten pool.

4.2 Porosity analysis

Porosity was identified within the deposited bead. While the AA4043 alloy exhibits low susceptibility to hot cracking, the deposit instead showed relatively large and numerous pores. Pore diameters predominantly ranged between 23 and 60 micrometers, with some reaching up to 90 micrometers; the largest measured 89.639 µm and the smallest 14.551 µm, while the average pore area was calculated as 79.379 µm². Porosity in WAAM-deposited beads typically arises from voids or gas pockets becoming trapped within the molten metal during deposition [92]. Mitigating such defects requires several approaches, most notably optimized gas shielding to limit atmospheric entrapment, along with precise regulation of welding parameters such as voltage, current, and wire feed speed to maintain a stable molten pool [93].

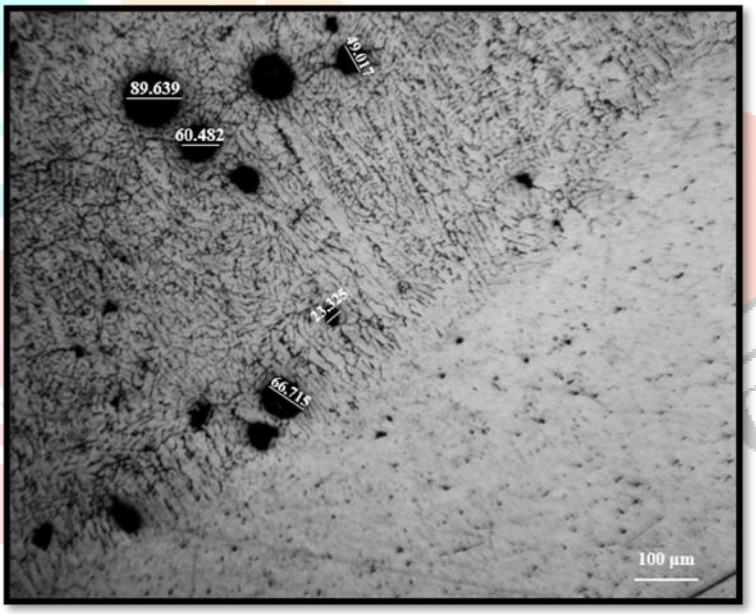

Figure3. Porosity defect in deposited bead.

4.3 XRD Phase Analysis

The X-ray diffraction (XRD) pattern of the wire arc additive manufactured (WAAM) ER-4043 aluminium alloy is shown in the provided Figure 18. The diffraction profile indicates that the deposited material predominantly consists of a **face-centred cubic (FCC) α-Al matrix**, together with minor intermetallic phases formed during solidification. The intense diffraction peaks located approximately at **2θ ≈ 38.5°, 44.7°, 65.1°, and 78.2°** can primarily be associated with the characteristic reflections of the α-Al phase. The strong intensity of the α-Al peaks confirms that aluminium constitutes the dominant crystalline phase in the deposited structure.

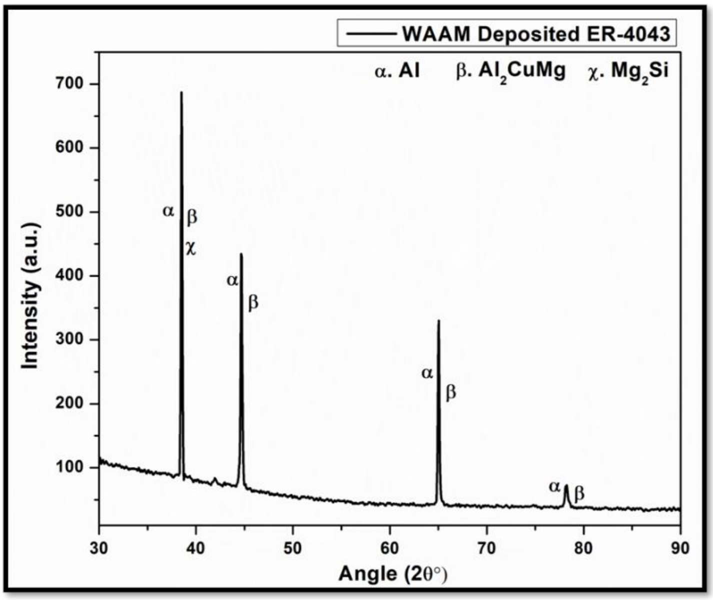

Figure 4. Analysed X-ray diffraction pattern of deposited bead of ER-4043 Aluminium alloy by using WAAM with robotic GMAW.

In addition to α-Al, relatively weak reflections corresponding to **β-Al_2CuMg** and **χ-Mg_2Si** phases are indicated in the XRD pattern. These secondary phases are likely associated with the alloying elements and their redistribution during the rapid, repeated melting and solidification cycles inherent to the WAAM process. The presence of Mg and Si-containing phases can influence the mechanical and corrosion behaviour of the deposited alloy. The comparatively lower intensity of the intermetallic peaks suggests that these phases are present in relatively small quantities compared with the α-Al matrix. Overall, the XRD analysis confirms that the WAAM ER-4043 deposit possesses an α-Al dominated matrix with minor intermetallic constituents, demonstrating the phase constitution developed during the WAAM deposition process.

4.4 Microhardness Analysis

Figure 5 illustrates the microhardness profile along the bottom-to-top direction of the ER-4043 aluminum alloy bead deposited via WAAM. Hardness was found to be elevated in specific regions of the deposit when a high tool travel speed and constant current were employed. This variation arises because the bottom of the bead, being in direct contact with the substrate, experiences a faster heat dissipation rate, whereas the top region cools more slowly. Consequently, the differing solidification rates and thermal gradients across the bead height produce a corresponding variation in microstructure, which in turn causes the observed change in microhardness from top to bottom.

Vickers microhardness testing of the AA4043 deposit was carried out using a diamond pyramid indenter under a controlled applied load, with hardness values derived from the measured diagonal lengths of the resulting indentations. Measurements taken across different zones of the bead revealed a consistent decreasing trend in hardness from the bottom to the top (76.6, 75.8, 75.6, and 73.9 HV, respectively), with an average hardness of 75.47 HV recorded across the deposit. This characterization approach proves valuable for evaluating the mechanical properties of the alloy and supports broader efforts in material quality assessment.

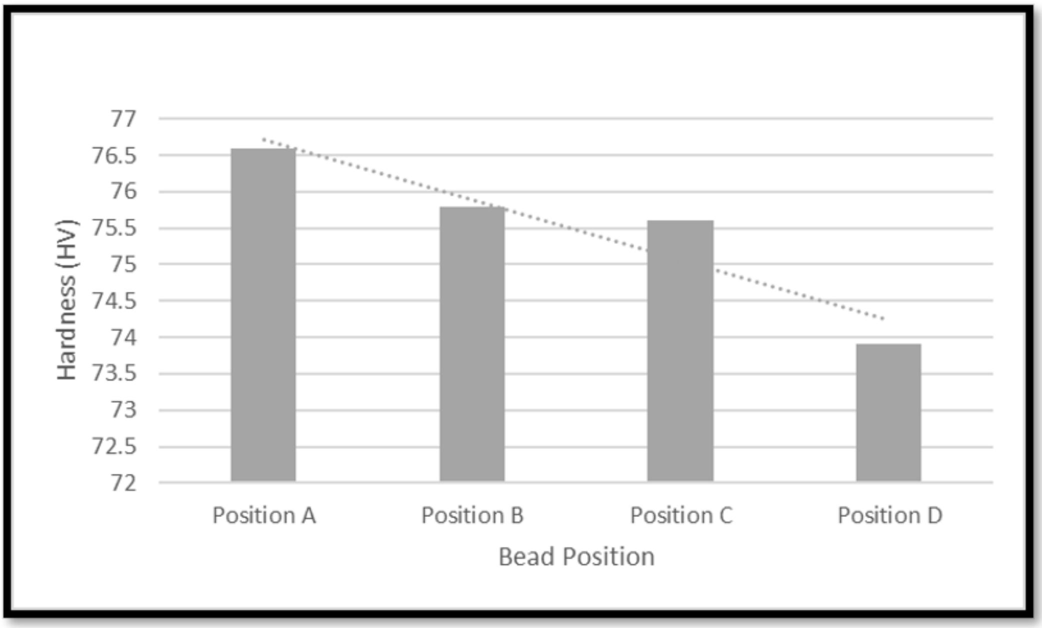

Figure 5. Variation of microhardness of deposited bead of ER 4043 aluminium

5.1 Conclusion

This study conducted mechanical and metallurgical characterization of the wall structure deposited using optimized process parameters. Hardness values were observed to vary along the bottom-to-top direction of the deposit. SEM analysis revealed a predominantly equiaxed grain structure, along with the presence of some porosity attributed to entrapped atmospheric oxygen. Based on these findings, the following conclusions were drawn:

(a) It is identified that the surface roughness as the most influential criterion affecting deposition quality, whereas toe angle had the least impact on the quality of WAAM-deposited beads.

(b) Alternative 15 emerged as the optimal deposition parameter set, yielding the lowest surface roughness alongside the highest toe angle, bead height, and depth of penetration.

(c) Porosity analysis of the bead deposited under optimal parameters revealed an average pore area of 79.379 μm^2. Pore diameters ranged predominantly between 23 and 60 micrometers, with the largest pore measuring close to 90 µm and the smallest measuring 14.551 µm.

(d) Cross-sectional micrographs of the ER-4043 aluminum alloy specimen, deposited at a travel speed of 4.5 mm/s, wire feed rate of 8.5 mm/s, and constant current of 50 A, were obtained using optical and scanning electron microscopy. The resulting microstructure exhibited features characteristic of Al-Si solidification, with the microstructural evolution of the deposited beads shown to be governed by the input process parameters.

(e) Microhardness testing across different zones of the bead cross-section revealed higher hardness values at the bottom of the specimen and lower values toward the top, with an average hardness of 75.47 HV recorded across the deposit.

6.1 References

1. L.E. Murr, S.M. Gaytan, D.A. Ramirez, E. Martinez, J. Hernandez,K.N. Amato, P.W. Shindo, F.R. Medina, R.B. Wicker, J.Mater. Sci. Technol. 28, 1 (2012)

2.Agarwala M, Bourell D, Beaman J, Marcus H, Barlow J. Direct selective laser sintering of metals. Rapid Prototyp J 1995;1:26–36.

3. A. Townsend, N. Senin, L. Blunt, R.K. Leach, J.S. Taylor, Precis.Eng. 46, 34 (2016)

4. L. Yuan, Z. Pan, D. Ding, Z. Yu, S. van Duin, H. Li, W. Li, J. Norrish, J. Manuf. Process, 65, 0–1 (2020). https://doi.org/10.1016/j.jmapro.2020.03.018

5. Mukherjee, S.: Laser Surface Modification of Ti6Al4V Implants. (2014).

6. Busachi A, Erkoyuncu J, Colegrove P, Martina F, Ding J. Designing a WAAM based manufacturing system for defense applications. Procedia CIRP 2015;37:48–53..

7. Ding J, Colegrove P, Mehnen J, Ganguly S, Sequeira Almeida PM, Wang F et al. Thermo-mechanical analysis of wire and arc additive layer manufacturing process on large multi-layer parts. Computational Materials Science 2011.

8. C. Zhang, M. Gao, X. Zeng, Workpiece vibration augmented wire arc additive manufacturing of high strength aluminum alloy, J. Mater. Process. Technol. 271 (2019) 85–92. doi:https://doi.org/10.1016/j.jmatprotec.2019.03.028.

9. D. Buchbinder, W. Meiners, N. Pirch, K. Wissenbach, J. Schrage, Investigation on reducing distortion by preheating during manufacture of aluminum components using selective laser melting, J. Laser Appl. 26 (2014) 012004. doi:10.2351/1.4828755.

10. A. Horgar, H. Fostervoll, B. Nyhus, X. Ren, M. Eriksson, O.M. Akselsen, Additive manufacturing using WAAM with AA5183 wire, J. Mater. Process. Technol. 259 (2018)

11. Li, X., Ding, S.: Interpersonal Interface System of Multimedia Intelligent English Translation Based on Deep Learning. Sci Program. 2022, (2022). https://doi.org/10.1155/2022/8027003.

12. S.G. Shabestari, H. Moemeni, Effect of copper and solidification conditions on the microstructure and mechanical properties of Al–Si–Mg alloys, J. Mater. Process. Technol.153–154(2004) 198. doi:https://doi.org/10.1016/j.jmatprotec.2004.04.302.

13. B.E. Carroll, T.A. Palmer, A.M. Beese, Anisotropic tensile behavior of Ti–6Al–4V components fabricated with directed energy deposition additive manufacturing, Acta Mater. 87 (2015) 309–320.

14. Azimi, S.M., Britz, D., Engstler, M., Fritz, M., Mücklich, F.: Advanced Steel Microstructural Classification by Deep Learning Methods. Sci Rep. 8, 2128 (2018). https://doi.org/10.1038/s41598-018-20037-5.

15. H. Wang, W. Jiang, J. Ouyang, R. Kovacevic, Rapid prototyping of 4043 Al-alloy parts by VP-GTAW, J. Mater. Process. Technol. 148 (2004) 93–102. doi:10.1016/j.jmatprotec.2004.01.058.

16. V.A. Popovich, E. V Borisov, A.A. Popovich, V.S. Sufiiarov, D. V Masaylo, L. Alzina, Functionally graded Inconel 718 processed by additive manufacturing: Crystallographic texture, anisotropy of microstructure and mechanical properties, Mater. Des. 114 (2017) 441–449.

17. Thampiriyanon, J., Laungsakulthai, K., Laokhen, P., Thongnak, S., Khumkoa, S.: A feasibility study on metallurgical slag classification by microstructure recognition. In: Materials (2020). https://doi.org/10.4028/www.scientific.net/MSF.1009.107.

18. B. Cong, J. Ding, S. Williams, Effect of arc mode in cold metal transfer process on porosity of additively manufactured Al-6.3%Cu alloy, Int. J. Adv. Manuf. Technol. 76 (2015) 1593–1606. doi:10.1007/s00170-014-6346-x.

19. J. Gu, J. Ding, S.W. Williams, H. Gu, P. Ma, Y. Zhai, The effect of inter-layer cold working and post-deposition heat treatment on porosity in additively manufactured aluminum alloys, J. Mater. Process. Technol. 230 (2016) 26–34. doi:10.1016/j.jmatprotec.2015.11.006.

20. J. Gu, J. Ding, S.W. Williams, H. Gu, J. Bai, Y. Zhai, P. Ma, The strengthening effect of inter-layer cold working and post-deposition heat treatment on the additively manufactured Al-6.3Cu alloy, Mater. Sci. Eng. A. 651 (2016) 18–26. doi:10.1016/j.msea.2015.10.101.
21. H. Geng, J. Li, J. Xiong, X. Lin, F. Zhang, Optimization of wire feed for GTAW based additive manufacturing, J. Mater. Process. Technol. 243 (2017) 40–47. doi:10.1016/j.jmatprotec.2016.11.027.
22. P.N. Anyalebechi, Analysis of the effects of alloying elements on hydrogen solubility in liquid aluminum alloys, Scr. Metall. Mater. 33 (1995) 1209–1216.
23. S. Kou, Y. Le, Alternating grain orientation and weld solidification cracking, Metall. Trans. A. 16 (1985) 1887–1896.24. Lai, C., Song, L., Han, Y., Li, Q., Gu, H., Wang, B., Qian, Q., Chen, W.: Material image segmentation with the machine learning method and complex network method. In: MRS Advances (2019). https://doi.org/10.1557/adv.2019.7.
24. D. Buchbinder, W. Meiners, N. Pirch, K. Wissenbach, J. Schrage, Investigation on reducing distortion by preheating during manufacture of aluminum components using selective laser melting, J. Laser Appl. 26 (2014) 012004. doi:10.2351/1.4828755.
25. C.A. Brice, W.H. Hofmeister, Determination of bulk residual stresses in electron beam additive-manufactured aluminum, Metall. Mater. Trans. A Phys. Metall. Mater. Sci. 44 (2013) 5147–5153. doi:10.1007/s11661-013-1847-z.
26. Liao, T.W.: Improving the accuracy of computer-aided radiographic weld inspection by feature selection. NDT and E International. 42, (2009). https://doi.org/10.1016/j.ndteint.2008.11.002.
27. Choudhary, K., DeCost, B., Chen, C., Jain, A., Tavazza, F., Cohn, R., Park, C.W., Choudhary, A., Agrawal, A., Billinge, S.J.L., Holm, E., Ong, S.P., Wolverton, C.: Recent advances and applications of deep learning methods in materials science, (2022). https://doi.org/10.1038/s41524-022-00734-6.
28. Yasuda, T., Ookawara, S., Yoshikawa, S., Matsumoto, H.: Machine learning and data-driven characterization framework for porous materials: Permeability prediction and channeling defect detection. Chemical Engineering Journal. 420, (2021). https://doi.org/10.1016/j.cej.2021.130069.
29. F. Fina, A. Goyanes, S. Gaisford, A.W. Basit, Selective laser sintering (SLS) 3D printing of medicines, Int. J. Pharm. 529 (1–2) (2017) 285–293 .
30. S. Vijayavenkataraman, J.Y.H. Fuh, W.F. Lu, 3D printing and 3D bioprinting in pediatrics, Bioengineering 4 (3) (2017) 63 .
31. J.W. Stansbury, M.J. Idacavage, 3D printing with polymers: challenges among expanding options and opportunities, Dent. Mater. 32 (1) (2016) 54–64 .32.Wijesinghe, K., Wanni, J., Banerjee, N.K., Banerjee, S., Achuthan, A.: Characterization of microscopic deformation of materials using deep learning algorithms. Mater Des. 208, (2021). https://doi.org/10.1016/j.matdes.2021.109926.
32. J. Suwanprateeb, S. Kerdsook, T. Boonsiri, P. Pratumpong, Evaluation of heat treatment regimes and their influences on the properties of powder-printed high-density polyethylene bone implant, Polym. Int. 60 (5) (2011) 758–764 .
33. Ríos S, Colegrove PA, Martina F, Williams SW (2018) Analytical process model for wire + arc additive manufacturing. Addit Manuf 21:651–657. https://doi.org/10.1016/j.addma.2018.04.003
34. Ahsan MRU, Tanvir ANM, Seo GJ et al (2020) Heat-treatment effects on a bimetallic additively-manufactured structure (BAMS) of the low-carbon steel and austenitic-stainless steel. Addit Manuf, https://doi.org/10.1016/j.addma.2020.101036
35. Ding D, Pan Z, Cuiuri D, Li H (2015) Wire-feed additive manufacturing of metal components: technologies, developments and future interests. Int J Adv Manuf Technol 81:465–481. https://doi.org/10.1007/s00170-015-7077-3
36. Walambe, R., Marathe, A., Kotecha, K.: Multiscale object detection from drone imagery using ensemble transfer learning. Drones. 5, (2021). https://doi.org/10.3390/drones5030066.
37. Ali Y, Henckell P, Hildebrand J, Reimann J, Bergmann JP, Barnikol-Oettler S (2019) Wire arc additive manufacturing of hot work tool steel with CMT process. J Mater Process Technol 269:
109–116. https://doi.org/10.1016/j.jmatprotec.2019.01.034

38. Xu X, Ding J, Ganguly S, Diao C, Williams S (2018) Preliminary investigation of building strategies of maraging steel bulk material using wire + arc additive manufacture. J Mater Eng Perform 28:1–7. https://doi.org/10.1007/s11665-018-3521-5
39. Zhao H, Zhang G, Yin Z, Wu L (2011) A 3D dynamic analysis of thermal behavior during single-pass multi-layer weld-based rapid prototyping. JMater Process Technol 211:488–495. https://doi.org/10.1016/j.jmatprotec.2010.11.002
40. B. Wu, Z. Pan, D. Ding, D. Cuiuri, H. Li, J. Xu, J. Norrish, J.Manuf. Process. 35, 127 (2018)
41. Sachlos E, Czernuszka J T. Making tissue engineering scaffolds work. Review: the application of solid freeform fabrication technology to the production of tissue engineering scaffolds.European Cells & Materials, 2003, 5: 29–39, discussion 39–40
42. Tan, Y., Wang, X., Kang, Z., Ye, F., Chen, Y., Zhou, D., Zhang, X., Gong, J.: Creep lifetime prediction of 9% Cr martensitic heat-resistant steel based on ensemble learning method. Journal of Materials Research and Technology. 21, (2022). https://doi.org/10.1016/j.jmrt.2022.11.067.
43. Onuh S O, Yusuf Y Y. Rapid prototyping technology: applications and benefits for rapid product development. Journal of Intelligent Manufacturing, 1999, 10(3/4): 301–311
44. van Dyk, D.A., Meng, X.-L.: The Art of Data Augmentation. Journal of Computational and Graphical Statistics. 10, 1–50 (2001). https://doi.org/10.1198/10618600152418584.
45. Zhang W, Leu M C, Ji Z, Yan Y. Rapid freezing prototyping with water. Materials & Design, 1999, 20(2–3): 139–145
46. Liu Q, Sui G, Leu M C. Experimental study on the ice pattern fabrication for the investment casting by rapid freeze prototyping. Computers in Industry, 2002, 48(3): 181–197
47. Luengo, J., Moreno, R., Sevillano, I., Charte, D., Peláez-Vegas, A., Fernández-Moreno, M., Mesejo, P., Herrera, F.: A tutorial on the segmentation of metallographic images: Taxonomy, new MetalDAM dataset, deep learning-based ensemble model, experimental analysis and challenges, (2022). https://doi.org/10.1016/j.inffus.2021.09.018.
48. Bryant F D, Sui G, Leu M C. A study on effects of process parameters in rapid freeze prototyping. Rapid Prototyping Journal,2003, 9(1): 19–23
49. Monneret S, Loubere V, Corbel S. Microstereolithography using dynamic mask generator and a non-coherent visible light source. Proceedings of the Society for Photo-Instrumentation Engineers, 1999, 3680: 553–561
50. Thomas C L, Gaffney T M, Kaza S, Lee C H. Rapid prototyping of large scale aerospace structures. In: Proceedings of Aerospace Applications Conference IEEE. Aspen, CO, 1996, 4: 219–230
51. Sun C, Fang N, Wu D M, Zhang X. Projection micro-stereolithography using digital micro-mirror dynamic mask.Sensors and Actuators. A, Physical, 2005, 121(1): 113–120
52. Waterman N A, Dickens P. Rapid product development in the USA, Europe and Japan. World Class Design to Manufacture, 1994, 1(3): 27–36
53. Arif, E., Shahzad, S.K., Iqbal, M.W., Jaffar, M.A., Alshahrani, A.S., Alghamdi, A.: Automatic Detection of Weapons in Surveillance Cameras Using Efficient-Net. Computers, Materials and Continua. 72, (2022). https://doi.org/10.32604/cmc.2022.027571.
54. Mazumder J, Dutta D, Kikuchi N, Ghosh A. Closed loop direct metal deposition: art to part. Opt Lasers Eng 2000;34:397–414
55. Zhang, T., Zhang, X., Ke, X.: Quad-fpn: A novel quad feature pyramid network for sar ship detection. Remote Sens (Basel). 13, (2021). https://doi.org/10.3390/rs13142771.
56. Filippo Montevecchi, Niccolò Grossi, Hisataka Takagi, Antonio Scippa, Hiroyuki Sasahara, Gianni Campatelli, Cutting Forces Analysis in Additive Manufactured AISI H13 Alloy, Procedia CIRP, Volume 46,2016, Pages 476-479, ISSN 2212-8271, http://dx.doi.org/10.1016/j.procir.2016.04.034.
57. B. Wu, D. Ding, Z. Pan, D. Cuiuri, H. Li, J. Han, Z. Fei, J. Mater. Process. Tech. 250, 304 (2017)
58. T. Abe, H. Sasahara, Precis. Eng. 45, 387 (2016)
59. Y. Yehorov, L.J. da Silva, A. Scotti, J. Manuf. Mater. Process. 3,32 (2019)

60. L. Yuan, Z. Pan, D. Ding, F. He, S. van Duin, H. Li, W. Li,Robot. Comput. Integr. Manuf. 63, 101916 (2020)

61. L. Yuan, Z. Pan, D. Ding, Z. Yu, S. van Duin, H. Li, W. Li, J. Norrish, J. Manuf. Process, 65, 0–1 (2020). https://doi.org/10.1016/j.jmapro.2020.03.018

62. W. Ou, Y. Wei, R. Liu, W. Zhao, J. Cai, J. Manuf. Process. 53,84 (2020)

63. D. Wu, X. Hua, D. Ye, F. Li, Int. J. Heat Mass Tran. 104, 634 (2017)

64. B. Cong, J. Ding, S. Williams, Effect of arc mode in cold metal transfer process on porosity of additively manufactured Al-6.3%Cu alloy, Int. J. Adv. Manuf. Technol. 76 (2015) 1593–1606. doi:10.1007/s00170-014-6346-x.

65. R. Manti, D.K. Dwivedi, A. Agarwal, Microstructure and hardness of Al-Mg-Si weldments produced by pulse GTA welding, Int. J. Adv. Manuf. Technol. 36 (2008) 263–269.

66. M. R. Dunlavey, "Efficient polygon-filling algorithms for raster displays," ACM Transactions on Graphics (TOG), vol. 2, pp. 264-273, 1983.

67. V. Rajan, et al., "The optimal zigzag direction for filling a two-dimensional region," Rapid Prototyping Journal, vol. 7, pp. 231-241, 2001.

68. H. Li, et al., "Optimal toolpath pattern identification for single island, sculptured part rough machining using fuzzy pattern analysis," Computer-Aided Design, vol. 26, pp. 787-795, 1994.

69. P. Kulkarni, et al., "A review of process planning techniques in layered manufacturing," Rapid Prototyping Journal, vol. 6, pp. 18-35, 2000.

70. W. Chiu, et al., "Toolpath generation for layer manufacturing of fractal objects," Rapid Prototyping Journal, vol. 12, pp. 214-221, 2006.

71. T. Wasser, et al., "Implementation and evaluation of novel buildstyles in fused deposition modeling (FDM)," Strain, vol. 5, p. 6, 1999.

72. Heimann, R.B. Silicon Nitride, a Close to Ideal Ceramic Material for Medical Application. Ceramics 2021, 4, 208–223.

73. Perrichon, A.; Reynard, B.; Gremillard, L.; Chevalier, J.; Farizon, F.; Geringer, J. A testing protocol combining shocks, hydrothermal ageing and friction, applied to Zirconia Toughened Alumina (ZTA) hip implants. J. Mech. Behav. Biomed. Mater. 2017, 65, 600–608.

74. Harnpornchai, N.; Wonggattaleekam, W. An Application of Neutrosophic Set to Relative Importance Assignment in AHP. Mathematics 2021, 9, 2636.

75. Singh, T.; Patnaik, A.; Fekete, G.; Chauhan, R.; Gangil, B. Application of hybrid analytical hierarchy process and complex proportional assessment approach for optimal design of brake friction materials. Polym. Compos. 2019, 40, 1602–1608.

76. Brodny, J.; Tutak, M. Analyzing the Level of Digitalization among the Enterprises of the European Union Member States and Their Impact on Economic Growth. J. Open Innov. Technol. Mark. Complex. 2022, 8, 70.

77. Sood, A.K., R.K. Ohdar, and S.S. Mahapatra. 2009. Improving dimensional accuracy of fused deposition modelling processed part using grey Taguchi method. Materials and Design 30:4243–4252.

78. Zhang, J., and A. Peng. 2012. Process-parameter optimization for fused deposition modeling based on Taguchi method. Advanced Materials Research 538: 444–447.

79. Kumar, D., V.N. Kannan, and G. Sankaranarayanan. 2014. Parameter optimization of ABS-M30i parts produced by fused deposition modeling for minimum surface roughness. International Journal of Current Engineering and Technology 3: 93–97.

80. Wang, C.C., Ta-Wei Lin, and Shr-Shiung Hu. 2007. Optimizing the rapid prototyping process by integrating the Taguchi method with the Gray relational analysis. Rapid Prototyping Journal 13 (5): 304–315.

81. Srivastava, M., M. Sachin, T.K. Kundra, and R. Sandeep. 2017. Multi-response optimization of fused deposition modelling process parameters of ABS using response surface methodology (RSM)-based desirability analysis. Materials Today: Proceedings 4: 1972–1977.

82. Abdullaha, A., D. Mohamada, T.N. Rahim, H.M. Akil, and Z.A. Rajiona. 2015. 3d printer's parameter optimization for potential patient specific implant fabrication. Jurnal Teknologi 76(7): 75–79.
83. Alhubail, M., D. Alenezi, and B. Aldousiri. 2013. Taguchi-based optimization of process parameters of fused deposition modelling for improved part quality. International Journal of Engineering Research and Technology 2 (12): 2519.
84. Thrimurthulu, K., M.P. Pulak, and N.Venkata Reddy. 2004. Optimum part deposition orientation in fused deposition modeling. International Journal of Machine Tools and Manufacture 44:585–594.
85. Nidagundi, V.B., R. Keshavamurthy, and C.P.S. Prakash. 2015. Studies on parametric optimization for fused deposition modelling process. Materials Today: Proceedings 2:1691–1699.
86. C. Dharmendra, A. Hadadzadeh, B.S. Amirkhiz, G.D. Janaki Ram, M. Mohammadi, Microstructural evolution and mechanical behavior of nickel aluminum bronze Cu-9Al-4Fe-4Ni-1Mn fabricated through wire-arc additive manufacturing, Addit. Manuf. 30 (2019), 100872.
87. Nie Y, Zhang P, Wu X, Li G, Yan H, Yu Z (2018) Rapid prototyping of 4043 Al-alloy parts by cold metal transfer. Sci Technol Weld Join 23:527–535
88. A. G. Ortega et al., "Characterisation of 4043 aluminum alloy deposits obtained by wire and arc additive manufacturing using a Cold Metal Transfer process," Science and Technology of Welding and Joining, vol.24, no. 6, pp. 538–547, 2019.
89. G. Langelandsvik, A. Horgar, T. Furu, H. J. Roven, and O. M. Akselsen, "Comparative study of eutectic Al-Si alloys manufactured by WAAM and casting," The International Journal of Advanced Manufacturing Technology, vol. 110, no. 3–4, pp. 935–947, 2020.
90. R. Pramod, S. M. Kumar, B. Girinath, A. R. Kannan, N. P. Kumar, and N. S. Shanmugam, "Fabrication, characterisation, and finite element analysis of cold metal transfer–based wire and arc additive–manufactured aluminum alloy 4043 cylinder," Welding in the World,vol. 64, no. 11, pp. 1905–1919, 2020.
91. Z. qiang Liu, P. lei Zhang, S. wei Li, D. Wu, and Z. shui Yu, "Wire and arc additive manufacturing of 4043 Al alloy using a cold metal transfer method," International Journal of Minerals, Metallurgy, and Materials, vol. 27, no. 6, pp. 783–791, 2020.